Earth and Planetary Science Letters 308 (2011) 284–297

Contents lists available at ScienceDirect

Earth and Planetary Science Letters

journal homepage: www.elsevier.com/locate/epsl

Pulverized fault rocks and damage asymmetry along the Arima-Takatsuki Tectonic Line, Japan

T.M. Mitchell [a,*], Y. Ben-Zion [b], T. Shimamoto [c,1]

[a] Experimental Geophysics Laboratory, Institute for Geology, Mineralogy, and Geophysics, Ruhr-University Bochum, D-44780, Bochum, Germany
[b] University of Southern California, Department of Earth Sciences, Los Angeles, CA 90089-0740, USA
[c] Department of Earth and Planetary Systems Science, Graduate School of Science, Hiroshima University, 1-3-1 Kagami-yama, Higashi-Hiroshima, 739-8526, Japan

ARTICLE INFO

Article history:
Received 16 August 2010
Received in revised form 21 March 2011
Accepted 12 April 2011
Available online 25 June 2011

Editor: P. Shearer

Keywords:
fault structure
pulverized rocks
asymmetric damage zone
dynamic fracturing

ABSTRACT

We present field and laboratory data on pulverized rocks at the Hakusui-kyo outcrop of the Arima-Takatsuki Tectonic Line (ATTL), which is a dextral strike slip fault with ~17 km displacement juxtaposing granite to the south against rhyolite to the north. The majority of slip at the surface is localized to a clay-rich gouge fault core 8–10 cm in width, surrounded by a coarsening outwards fault breccias up to 3 m wide. Fault damage is highly asymmetric with respect to the slipping zone. The granite south of the fault has a pulverized damage zone up to 200 m wide, while the rhyolite to the north has only about 3 m wide non-pulverized fault breccia. The degree of pulverization in the granite decreases approximately logarithmically with normal distance from the slip zone. The highly fractured pulverized rocks exhibit several distinct textural characteristics. In thin section, grains appear to be highly comminuted but the original grain shapes and margins are recognizable. Microfractures tend to be tensile in no preferred orientation. Grain fragments display little to no rotation and lack evidence of in-situ shear. Consequently, at macroscale the rocks appear to preserve original granitic textures, despite being highly fractured and friable. The observed pulverization and rock damage asymmetry are most consistent with generation mechanism involving ruptures on a bimaterial interface with statistically preferred propagation direction, leading to damage primarily on the side with higher seismic velocity at depth. This is supported by laboratory measurements of P-wave ultrasonic velocities on intact samples which indicate that the granites have consistently higher velocity than the rhyolite with increasing confining pressure.

1. Introduction

In recent years, 'pulverized fault zone rocks' have been studied and described along various sections of the San Andreas fault (Brune, 2001; Dor et al., 2006a, 2006b; Dor et al., 2009; Rockwell et al., 2009; Wilson et al., 2005), Garlock fault (Rockwell et al., 2009), San Jacinto fault (Dor et al., 2006b; Wechsler et al., 2009) and North Anatolian fault (Dor et al., 2008). These rocks are unique in comparison to other fault rocks in that they appear to have been shattered in situ, have very fine grain size, yet do not appear to have been subjected to significant shear strain. In addition, the pulverized rocks and other intense fault damage products were shown in previous studies to be strongly asymmetric with respect to the principal slip zone, residing primarily on the side with higher seismic velocity at depth.

Several authors suggested that pulverized fault zone rocks are of coseismic origin. Brune (2001) argued that vibrations of normal stress created from sliding on a rough fault during earthquakes at seismogenic depth may be the basic generation mechanism. In this case, near-fault rocks may be subjected to rapid drops of confining pressure during successive earthquake ruptures, repeatedly fracturing the rock mass to very fine grain sizes without clear apparent shear. This process is expected to produce a damage zone that is approximately symmetric with respect to the main sliding surface. Ben-Zion and Shi (2005) suggested, based on simulations of dynamic ruptures with off-fault plastic yielding, that strongly asymmetric damage zones are the cumulative product of earthquake ruptures on bimaterial faults separating different elastic bodies. In such cases there is strong asymmetry in the dynamic strain fields at the rupture tips propagating in the opposite along-strike directions (e.g. Ben-Zion, 2001; Weertman, 1980), leading for various conditions to a statistically preferred rupture direction and strong reduction of normal stress near the propagating tip (e.g., Ampuero and Ben-Zion, 2008; Ben-Zion and Andrews, 1998; Brietzke et al., 2009; Dalguer and Day, 2009; Shi and Ben-Zion, 2006). Repeating occurrences of such ruptures is expected to produce strongly asymmetric rock damage with properties consistent overall with the locations and macroscopic observations reported in previous studies of pulverized rocks. Doan

* Corresponding author.
E-mail address: tom.m.mitchell@btinternet.com (T.M. Mitchell).
[1] Now at State Key Laboratory of Earthquake Dynamics, Institute of Geology, China Earthquake Administration, P. O. Box 9803, Beijing 100029, China.

0012-821X/$ – see front matter © 2011 Elsevier B.V. All rights reserved.
doi:10.1016/j.epsl.2011.04.023

and Gary (2009) demonstrated with laboratory experiments that generation of pulverized rock may require very high strain rates (>150 s^{-1}) accommodated in very small strains, typical of pulverized rocks. They suggested that the high strain rates producing the observed pulverized rocks are generated by supershear ruptures. The proposed pulverization mechanisms are discussed further in Section 5.1.

To date, the only fault rock unambiguously viewed to be of coseismic origin is pseudotachylyte, a very fine grained fault rock generally agreed to be formed by frictional melting of fault wall rocks during rapid seismic slip (e.g. Sibson, 1975). Detailed studies of such rocks have previously been used to infer properties of earthquake rupture dynamics and source parameters (e.g. Di Toro et al., 2005a; Di Toro et al., 2005b). If pulverized rocks are indeed of coseismic origin then, as with pseudotachylytes, the analysis of such rocks can be used to make important observations on damage generated by coseismic processes. An improved understanding of the generating mechanism can provide key information on earthquake physics, in-situ dynamic stress conditions and operating brittle rheology on the class of faults where pulverization is observed. While the physical and chemical characteristics of pulverized rocks are beginning to be better understood, additional observations are needed to clarify the types of faults and lithologies where they may be observed and the generating mechanism.

In this paper we present and discuss new observations of pulverized rocks, along a strand of the Arima-Takatsuki Tectonic Line (ATTL) in Japan, and characterize the fault structure, damage distribution and textural features of the pulverized rocks. To provide additional constraints on the possible generating mechanism, we performed laboratory measurements of seismic velocities of intact undeformed host rock collected from around the fault zone and subjected to confining pressure conditions commensurate with pressures experienced by faults at depth. In light of these new observations, we assess which of the various generating mechanisms may be responsible for the creation of the observed pulverized rocks.

2. Previous observations on characteristics of pulverized rocks

Wilson et al. (2005) characterized pulverized rocks in a road cut exposure adjacent to the San Andreas fault (SAF) at Tejon Pass, following observations of Brune (2001) on the apparent lack of significant shear in the damage zone along the SAF at the Mojave and nearby regions. They showed that the pulverized rock formed a 70–100 m wide fault zone layer adjacent to the fault core where localized slip occurred. The main structure of this rock body was reported to consist of a multitude of small scale fractures and pervasive reduction of grain size, yet with a lack of macroscopic shear and retaining the original texture and crystal boundaries. Laboratory data suggest that the deformation is mechanical rather than chemical, due to a paucity of weathering products. Rockwell et al. (2009) presented a detailed analysis of chemical and physical characteristics of samples of pulverized Tejon Lookout Granite collected from various sections adjacent to the San Andreas and Garlock faults. Their X-Ray Diffraction analysis (XRD) confirmed minimal weathering products and that the breakdown process is primarily mechanical rather than chemical. They also showed in thin section analyses that at least some of the breakdown processes involved repeated tensile shattering in situ rather than shear dominated deformation. Pulverized rocks have very distinct characteristics separating them from typical fault zone rocks such as cataclasites, which experience localized shear, grain rolling/rounding and grain size reduction (e.g. Blenkinsop, 1991).

Dor et al. (2006a) mapped pulverized rocks at tens of sites along the entire (~140 km long) Mojave section of the SAF. They found that essentially all outcrops of crystalline rock within 100–300 m zone adjacent and parallel to the SAF are pulverized and lack macroscopic shear. They also showed that the pulverized rocks are present primarily on the side of the fault with higher seismic velocities at depth. From a variety of observations, Dor et al. (2006a) suggested that the observed pulverization may be a shallow phenomenon, having occurred in the top few kilometers of the crust. Dor et al. (2006b, 2008) documented strongly asymmetric pulverized and other damage products on scales ranging from centimeters to hundreds of meters in the structure of the San Jacinto fault near Anza, the Punchbowl fault, and several sections of the North Anatolia fault. Lewis et al. (2005) used seismic fault zone trapped waves to image the damage zone of the San Jacinto fault south of Anza on a scale of 100 m, and found a similar sense of damage asymmetry as was observed by the smaller scale geological mapping of Dor et al. (2006b). Wechsler et al. (2009) reported asymmetrical damage structures surrounding the San Jacinto Fault at a scale of 1 km, based on drainage density patterns inferred from analysis of geomorphic properties extracted from LiDAR and Shuttle Radar Topography Mission (SRTM) data. The region around Anza had more damage on the same side as in the observations of Dor et al. (2006b) and Lewis et al. (2005), while some regions further to the south had more damage on the opposite side. Lewis et al. (2007) inferred damage asymmetry in the structure of the SAF south of Hollister from inversions of fault zone head and direct *P* waves. The combined picture emerging from the forgoing observations is that fault zones hosting pulverized rocks have clear asymmetric damage with respect to the principal slip zone.

In the following sections we present results associated with a newly recognized outcrop of pulverized rock on the Arima-Takatsuki Tectonic Line, Japan.

3. Regional setting and general background to the ATTL

The southwestern area of Japan lies on the southeastern margin of the Eurasian plate, where the Philippine Sea plate is being subducted to the northwest beneath the Eurasian plate in the Nankai Trough. Plate convergence is at an oblique angle to the plate boundary in a direction N~50° ±5° W and at 40–50 mm/year (see Seno et al., 1993; Fig. 2a). A portion of this relative plate motion is accommodated by right-lateral strike slip faulting along a major east–northeast trending fault known as the Median Tectonic Line (MTL) located immediately south of Awaji Island and Osaka Bay, and is the most extensive structural boundary and active fault system in Japan (Fig. 1a).

The epicenter of the magnitude 7.2 Kobe earthquake occurred along the northeast-trending Nojima fault in Awaji Island and the Rokko fault system in Kobe, both major active faults in southwest Japan. The Arima-Takatsuki Tectonic Line (ATTL) strikes in an ENE–WSW direction, nearly parallel to the MTL (Fig. 1b). All of these faults, like the MTL, have a predominantly right-lateral strike-slip sense of displacement and constitute one of the most active fault systems in Japan (The Research Group for Active Faults of Japan, 1991). The ATTL is characterized by a linear fault zone and steep fault surfaces, and as with many active faults in the region, the main fault trace marks a topographic boundary between the mountainous regions and the basin which is easily seen in Landsat images (see Maruyama and Lin, 2002; Figs. 2a, 3a and 4a) and Bouguer gravity anomaly contour maps (Maruyama and Lin, 2002; Fig. 5). Along the eastern range-front segment, the ATTL offsets the late Pleistocene to Holocene fluvial terraces and alluvial fans from a few meters to a few tens of meters dextrally and vertically (Sangawa, 1978). Based on the offsets of age-estimated terraces, the average slip rate for the eastern range-front segment of the ATTL is estimated to be 0.5–1.5 mm/year dextrally and 0.1–0.8 mm/year vertically during the late Quaternary period (Sangawa, 1978). Total displacement along the ATTL has been inferred as ca. 16–18 km of right-lateral offset by restoring pre-Neogene sedimentary rocks along the fault (Maruyama and Lin, 2002; Fig. 2). Basement rocks in the study region consist mainly of the Triassic–Jurassic Tamba sedimentary complex, late Cretaceous felsic volcanic rocks of the

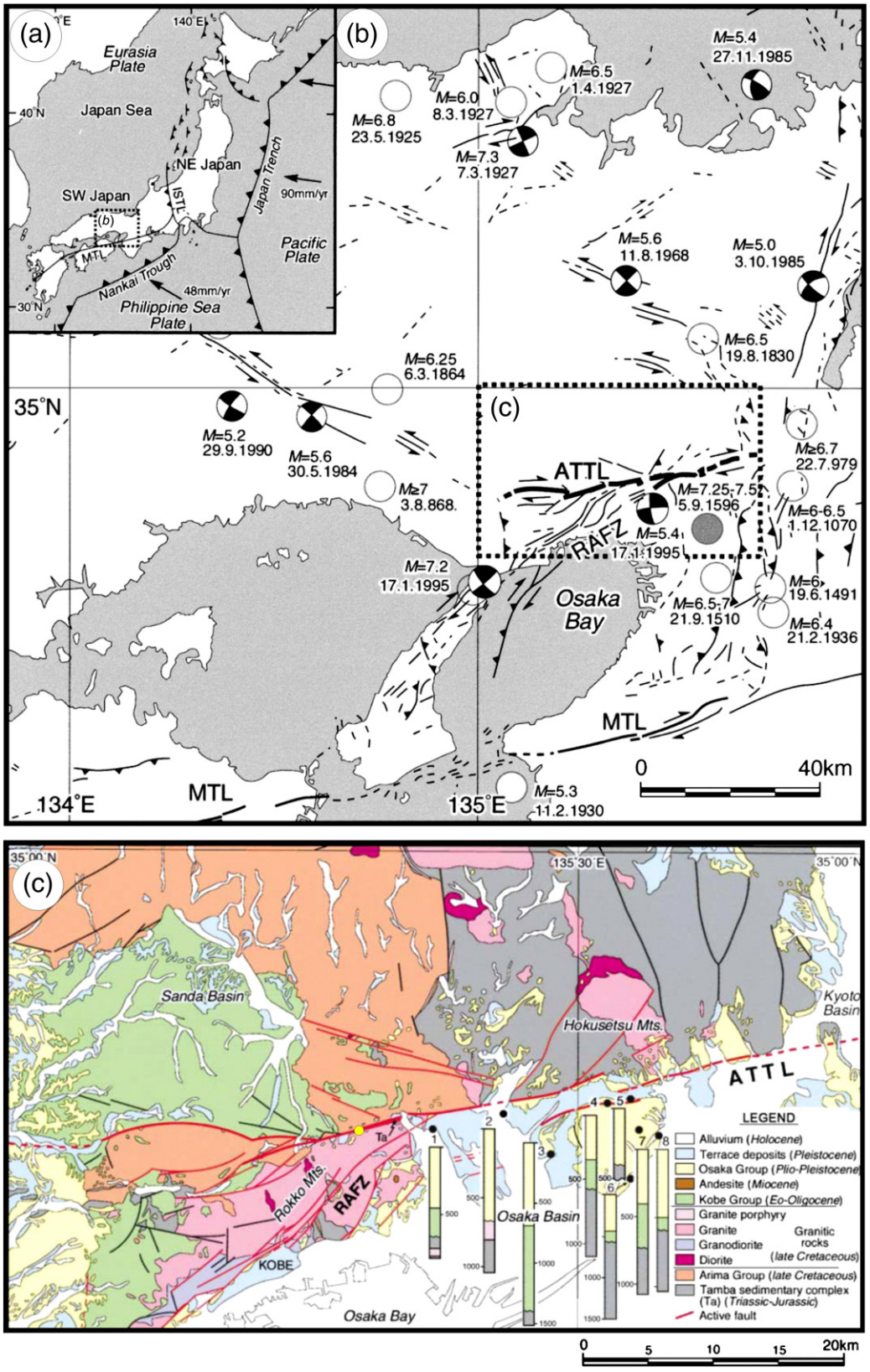

Fig. 1. (a) Index map showing current plate tectonic setting of Japan. From Maruyama and Lin (2002). (b) Map of major active faults and seismicity in southwest Japan. Active faults are derived mainly from Research Group for Active Faults of Japan (1991), from Maruyama and Lin (2002). (c) Geologic map along the ATTL from Maruyama and Lin (2002). Yellow circle marks the location of the Hakusui-Kyo outcrop.

Arima Group and granitic rocks and late Eocene to early Oligocene non-marine sedimentary rocks with rhyolitic tuff layers of the Kobe Group (e.g. Huzita and Kasama, 1982, 1983; Ozaki et al., 1996).

We now present detailed observations on a strand of the Arima-Takatsuki Tectonic Line (ATTL) called the Rokko fault, at a large outcrop exposed at Hakusui-Kyo, 2 km east of the town of Arima (Fig. 1).

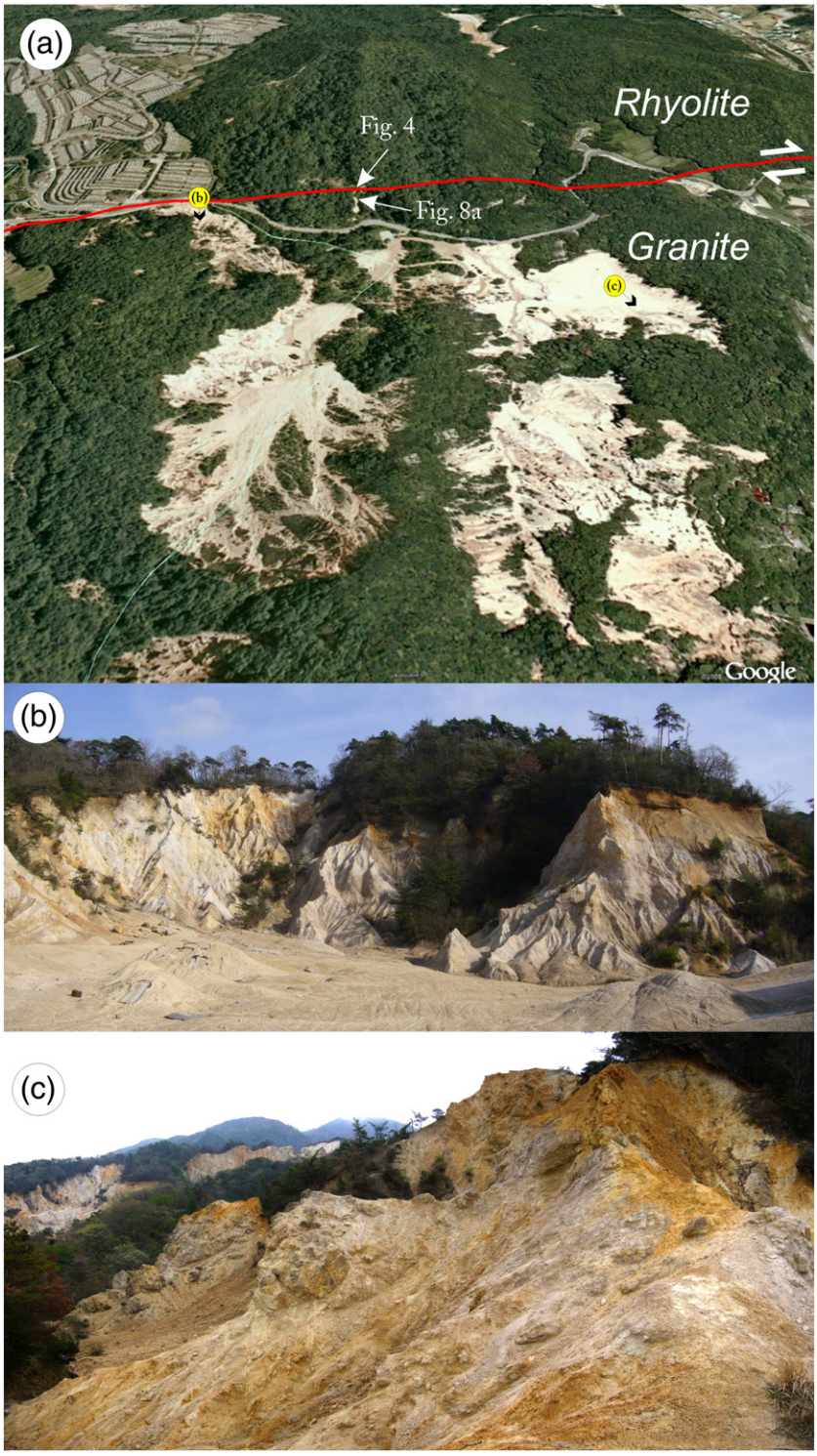

Fig. 2. (a) Google Earth image of the topographic outcrop of the Hakusui-Kyo outcrop of the ATTL. (b), (c) Examples of typical badlands-style topography of the Hakusui-Kyo outcrop of pulverized rocks. The locations where photographs were taken are marked in (a), with an arrow showing the direction of the view.

4. Observations

4.1. Approach

In order to characterize the fault structure, damage distribution and textural characteristics, detailed sampling transects were completed normal to the main fault trace of the ATTL. Samples were collected at a variety of distances from the core outwards into the damage zone in order to further understand the spatial variability of fault damage away from the fault. The spacing between samples was based on locations where good in-situ examples could be find; this ranged from 5 to 20 m spacing for the first 200 m of the transect, then 50 m to several hundred meters at greater distances. At each observation location, samples were taken for thin sectioning so that microfracture densities could be measured under the microscope, microstructural analysis and XRD analysis. Intact samples of pristine

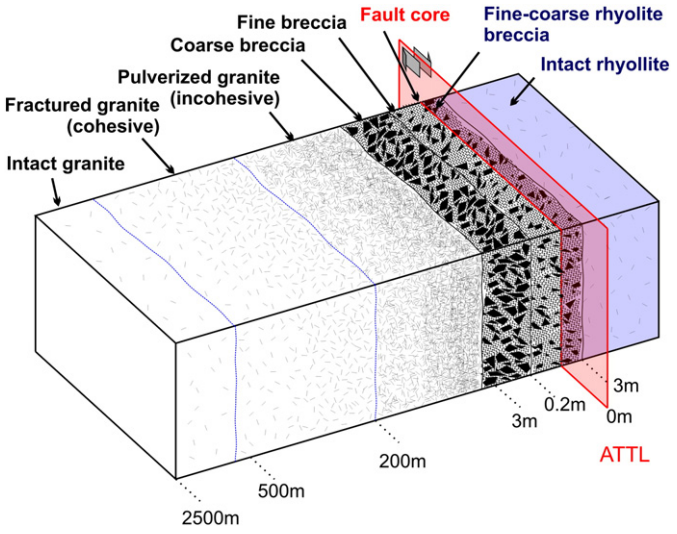

Fig. 3. Schematic diagram of the strongly asymmetric damage structure on the ATTL at the Hakusui-Kyo outcrop.

host rock were collected from both sides of the fault, outside of the fault zone, in order to measure seismic velocities in the laboratory.

To determine the microfracture density, methods similar to those described by Anders and Wiltschko (1994) and Wilson et al. (2003) were used. Fifty evenly spaced quartz grains per sample were analyzed. Thin sections were cut perpendicular to the fault plane and parallel to the slip direction, and as such any differences in measurements between the sections should reflect real variations in the fracture density. The microfracture density was determined by counting the number of microfractures that intersected a line of length 1.5 times the average grain diameter (Wilson et al., 2003). At each recording site consisting of randomly selected grains, the microscope stage was rotated an arbitrary amount in order to randomize the counting line orientation to minimize operator sampling bias. The total number of microfracture intersections was divided by the total counting line length to determine the average linear density of microfractures (Wilson et al., 2003). In addition to micro structural measurements, at all localities any subsidiary faults were recorded. We made basic observations of fault structure with increasing distance from the fault in order to define a schematic structure of the major parts of the fault damage.

4.2. Fault zone structure and damage distribution

At the Hakusui-Kyo outcrop, the Rokko Fault strand of the ATTL juxtaposes granite to the south against volcanic rock (rhyolite) to the north (Figs. 2a, 3, 4a,d). In the field, the topographic and morphological expression of the extent of fault damage is expressed in the granite outcrops which are characterized by Badlands-type erosion surfaces (Fig. 2). Such erosion surfaces are commonly seen in outcrops of pulverized rocks which may be indicative that the rock is fine grained and impermeable (e.g. Dor et al., 2006a), unlike the protolith at greater distances from the fault. The main fault core gouge zone is 8–10 cm in width and consists of dark-gray to brown clay-rich gouge (Figs. 3, 4d–f) and is likely to have hosted the majority of the fault's displacement, being the only very high strain product in the fault zone and separating the rhyolite and granitic bodies which have been displaced by up to 17 km (Maruyama and Lin, 2002). The fault core strikes approximately N88° W, dipping ~85° S. The contact between the gouge and granitic breccia is sharp (Fig. 4d). To the north of the core, a fault breccia consisting mainly of rhyolite fragments coarsens outwards over several meters into relatively intact rhyolite host rock (Fig. 4c). To the south, a fine-grained granitic breccia ~20 cm wide grades into a coarser breccia up to 3 m in width (Fig. 4b). The edge of the granitic fault breccia defines a boundary of the beginning of a large unit of highly damage incohesive fault rock, or pulverized rock. This pulverized rock extends approximately 200 m outwards to the south of the fault core (Fig. 3), although patches of relatively more cohesive rock exist within this zone. Beyond a distance of about 200 m, the granite is relatively cohesive yet still fractured, and this damage extends up to around 500–600 m from the fault (Fig. 3). Fault damage is clearly highly asymmetric with respect to the slipping zone: a several hundred-meter wide pulverized damage zone in the granite to the south of the fault, and a small non-pulverized damage zone consisting of fault breccia around 3 m in width in the rhyolites to the north.

Microfracture density as a function of distance from the ATTL fault core shows a striking damage asymmetry across the fault core (Fig. 5). Examples of microfractures measured can be seen in Fig. 6. After several meters into the rhyolite the microfractures appear to fall off from around 20/mm to apparently constant background levels of around 5–10/mm. In contrast, the microfracture densities in the granite are much higher, with densities around 80/mm close to the fault falling to around 20–40/mm after several hundred meters. The high microfracture densities correspond well with the zone of pulverized rock (Fig. 3); where fracturing is presumably so intense that the rock ceases to be cohesive. Beyond this boundary, microfracture densities fall off to background levels at distances greater than 550–600 m.

Along strike of the ATTL, there are occasional outcrops of badland-style topography in localized patches within the granitic rocks to the South of the ATTL. Good examples can be seen between the town of Arima all along to the ENE through Horai-kyo towards Takarazuka following the general strike of the ATTL. However, searches for such highly damaged rock in units on the north block of the ATTL within the rhyolite have proved unsuccessful. While further mapping needs to be completed to fully understand the extent of the pulverized rock outcrops, it appears that such pulverized outcrops appear limited to the granitic rocks.

4.3. Textural characteristics of ATTL pulverized rock

The highly microfractured pulverized rocks appear to exhibit distinct textural characteristics. Grains appear to be highly comminuted but the original grain shapes and margins are still recognizable under the naked eye (Fig. 6a and b) and in thin section (Fig. 6c, d and e). A general lack of in situ shear is demonstrated by microfractures which do not show significant offset of grain boundaries and feldspar twins. In addition, grain fragments (e.g. Fig. 6c) commonly show little to no rotation, as can be seen under cross polarized light (Fig. 6d) when crystals generally go extinct at the same time when the microscope stage is rotated. The lack of grain rotation and shearing imply that the comminution process was by an in situ tensile shattering mechanisms rather than shearing. Consequently, at macroscale the rocks seem to preserve original granitic textures, despite being highly microfractured and friable to the touch (Fig. 6a, b and f). Microfractures tend to be of opening mode (e.g. Fig. 6c and e), and generally cross the entire length of grains as intergranular fractures. Many of these microfractures are open relatively wide (arrowed in Fig. 6e) with no obvious preferred opening mode orientation, possibly indicating expansion and dilation. Scanning electron microscope (SEM) images of more intensely pulverized samples within meters to the fault core demonstrate an abundance of residual angular quartz fragments that are broken down to the range of 20–100 μ scale, and fragmentation of grains can occur down to the micron scale (Fig. 6h), even in samples at over 20 m away from the fault core. Relatively high levels of pervasive microfracturing can also be seen in samples as far as 150 m from the fault where samples are still highly friable (Fig. 6f). Quartz grains under the optical microscope

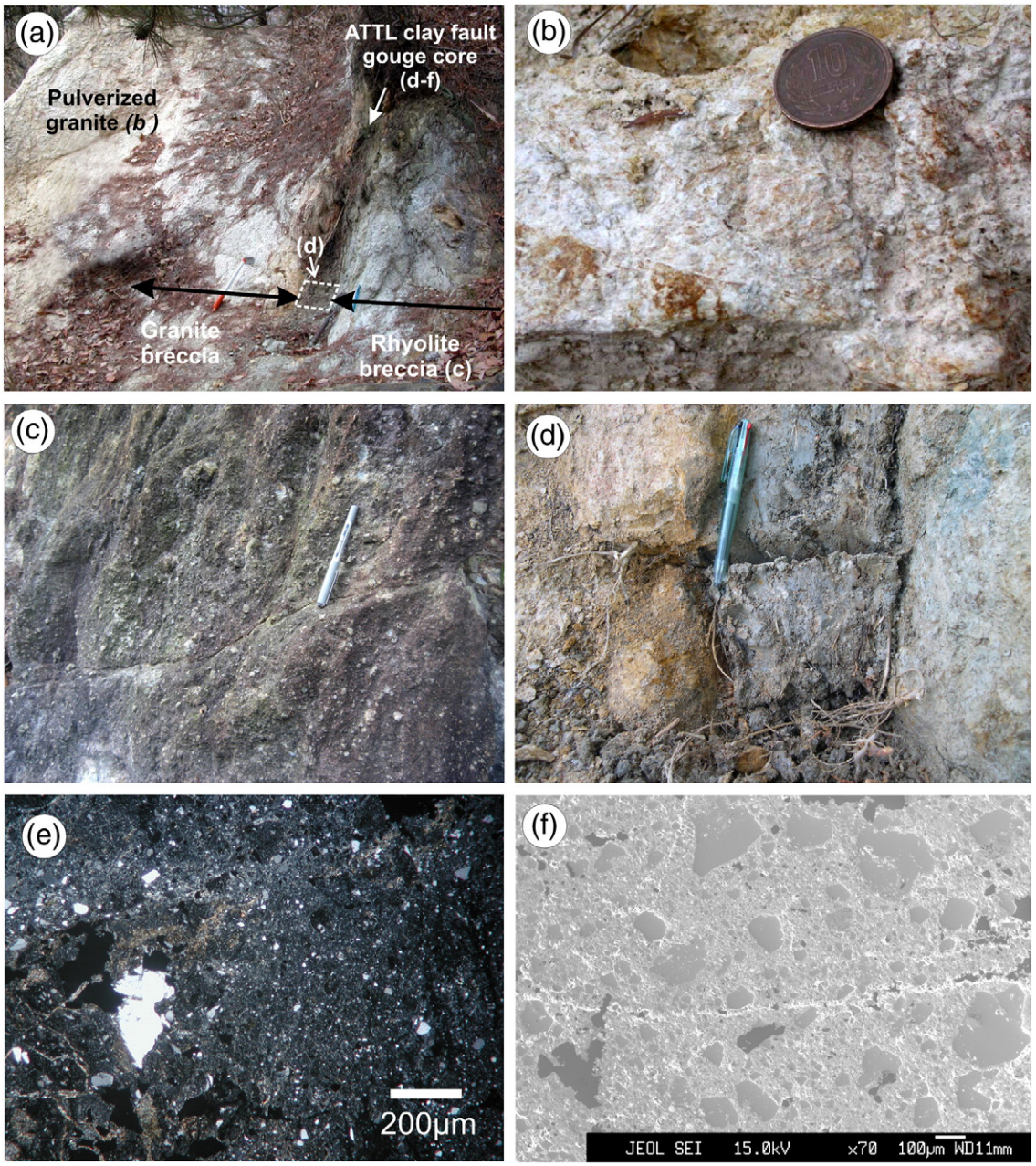

Fig. 4. (a) Outcrop of the fault core, breccias and pulverized rocks around the core zone of the ATTL. The location of the fault core shown in detail in (d) is marked. (b) Outcrop of the granite fault breccia to the south of the ATTL fault core. (c) Outcrop of the coarse rhyolite fault breccia to the north of the ATTL fault core. (d) Clayey fault gouge zone between the granite and rhyolite breccias. (e) Optical microscope image of the clayey fault gouge. (f) Scanning electron microscope secondary image of the clay fault gouge.

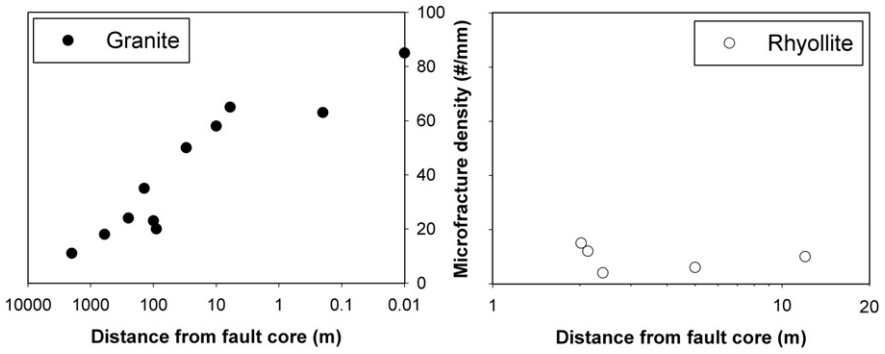

Fig. 5. Microfracture density versus perpendicular distance from the fault core for both sides of the ATTL in samples collected at different distances from the fault.

do not show evidence of any major dissolution; grains appear to be very angular in general rather than rounded, even in the most pulverized samples (Fig. 6g and h). There is little or no evidence of alteration to sericite along cracks, and while some plagioclase shows minor local breakdown to white mica and epidote, and K-feldspar to kaolinite, there is no obvious evidence of significant alteration.

4.4. Mineralogy

The fact that there is a clear spatial relationship of pulverization with distance from the fault zone suggests that the fracture damage is likely to be fault related. However, in order to rule out breakdown of the rock mass by weathering processes, we completed semi-quantitative XRD measurements on granite samples taken at distances of 2, 20 and 200 m from the fault core. The data shown in Fig. 7 clearly demonstrate that all three samples are similar in mineralogy.

At all three distances, quartz and feldspars dominate, and there is little biotite, muscovite, chlorite and kaolinite in the samples. Of the small amounts of phyllosilicates found, most consist of kaolinite and chlorite, and no amorphous material is present. These results, combined with optical microscopic observations showing little evidence of dissolution, suggest that the majority of the damage was mechanical rather than chemical, although there is some evidence for minor weathering and local breakdown. The absence of a change in mineralogy in the pulverized rock with increasing distance from the fault confirms that differential weathering is not the cause of variations in damage.

4.5. Subsidiary faulting and macroscopic fractures

While the bulk of the pulverized rock zone shows a preference for microfracture damage dominating and no localized shear, there are some pervasive macroscale fractures and subsidiary faults which crosscut the pulverized rocks (Fig. 8a and b). The largest subsidiary fault can be found about 10 m to the South of the fault core (Fig. 8a.), and despite no exposed displaced planar markers it is likely to have hosted several meters of slip owing to the presence of a fault core consisting of clayey gouge ranging up to 5 cm in thickness. Several other macroscopic faults crosscut the pulverized rock at various locations (e.g. Fig. 8b), showing small elements of localized shear and offset (Fig. 8c), all of which appear to host iron-rich vein material in their core (Fig. 8d). Natural occurring hot springs are common around the Arima area, coming to surface enriched in salt and iron (e.g. Teranishi et al., 2003). The hot springs in the region are probably the result of a compressional fault jog on the ATTL due to a slight bend in the fault trace, causing open fractures and increased permeability for fluid to travel upwards from depth. Widespread iron-rich veining around subsidiary faults may be due to similar natural hotspring water utilizing these zones as permeable pathways. Zones of localized shear deformation are generally restricted to areas in close proximity to the subsidiary faults. The level of pulverization neither increases nor decreases with proximity to these secondary fault features, suggesting that these features are late stage faulting events. In addition to this, some of these secondary faults displace highly pulverized rock against relatively less pulverized rock, indicating that the pulverization occurred prior to the faulting.

Orientations and spatial variation of localized faults range from shallow to steep orientations in typical shear orientations expected around a dextral fault; the summary stereonet of all orientation data shows that the dominant fault set varies from fault parallel to 30° clockwise to the main trace of the ATTL (Fig. 8e), in a Riedel orientation. Although looked for, there appears to be no major variation in subsidiary fault orientation with distance from the main ATTL trace.

4.6. Seismic velocity measurements under hydrostatic pressure

We conducted laboratory measurements on intact samples of granite and rhyolite collected from both sides of the fault (locations in Fig. 1), in order to determine seismic velocities of the rocks and to evaluate if velocity contrasts on either side of the fault in the intact host rock were consistent with models and observations predicting that asymmetric damage structures and shattered pulverized rocks on the high velocity side (Ben-Zion and Shi, 2005; Dor et al., 2006b; Dor et al., 2008). To measure seismic velocity in the samples, a high pressure intravessel triaxial apparatus with a permeameter and a simultaneous ultrasonic wave velocity measurement capability (Fig. 10) was used. This is a modification of the existing YOKO apparatus currently at the University of Hiroshima, Japan (Shimamoto, 2003), which enables the measurement of porosity, permeability and ultrasonic velocities simultaneously under hydrostatic conditions, although permeability and porosity are not considered here.

Ultrasonic wave velocities were made on cylindrical samples ~20 mm in diameter and 20 mm long jacketed in a polyolefin shrinkfit tube. A JSR DPR300 900 V pulser/receiver was used to excite a 1 MHz resonant frequency piezo-electric transmitting transducer, and this transducer was in direct contact with the sample (Fig. 9). Waveforms were captured from an identical receiver on the opposite sample end, and were pre-amplified and filtered on the pulser/receiver before being displayed and recorded on a digital oscilloscope. P-wave velocity measurements were subsequently performed under hydrostatic conditions using oil as a confining medium. The transducer assemblies were specially designed to be easily added or removed to the existing Yoko equipment (Fig. 9). The accuracy of the first arrivals gives errors of between 1 and 5%. Confining pressure was generated by a hydraulic pump and intensifier, and regulated with a pressure regulator.

Samples for velocity measurements were collected from outside the damage zones of the fault, at around 20 m from the fault core on the rhyolite and nearly a kilometer from the fault core in the granite. The P-wave velocity for the rhyolite ranges from 5.4 km/s at 10 MPa to 5.66 km/s at 100 MPa confining pressure (equivalent of 5 km depth), while the granite ranges from 5.5 km/s to nearly 5.9 km/s at 100 MPa. The P wave velocity for granite is consistently higher than that of the rhyolite for the range of confining pressures, and at greater pressures their velocities diverge and granite is significantly faster.

5. Discussion

We have described the basic fault zone structures, damage distribution and textural characteristics of rocks surrounding the Rokko strand of the ATTL, based on detailed microstructural and field observations. The ATTL hosts a significantly large unit of pulverized rock, found exclusively to the south of the fault in the granitic rock. The fault structure is highly asymmetric with respect to the slipping zone, as little damage is seen on the opposite side of the fault within the rhyolite. The damage asymmetry is also characterized quantitatively with microfracture density measurements, with granites showing fracture densities of 80/mm, compared to around 10–20/mm in the rhyolite at similar distances from the fault core. The observed damage asymmetry differs considerably from more symmetrical damage distributions found around some other strike-slip faults (e.g. Mitchell and Faulkner, 2009). The damage asymmetry agrees with previously documented various occurrences of pulverized rocks in localized exposed patches ranging up to 300 m in thickness from the core of large plate- or block-bounding strike-slip fault zones (e.g., the San Andreas and North Anatolian faults).

Fault-rock textures at the examined sites appear to share many similarities with existing well-documented observations of pulverized granitic rocks previously described in association with the San

Andreas, Garlock, and San Jacinto faults in southern California (Rockwell et al., 2009). All microscale observations appear to indicate that the rocks formed by some form of shattering mechanism, rather than more typical fault deformation involving mechanical breakdown by localized shear, grain rolling and grain size reduction, such as seen in cataclastic flow and brecciation (e.g. Blenkinsop, 1991; Sibson, 1977). The lack of in situ shear is supported by the fact that the most grains are angular and show no obvious offset. While some weathering products are present, this is only minor and no more than might be expected considering that samples were collected from surface derived samples. In addition, there is no change in mineralogy with increasing distance from the fault. We therefore conclude, as previous observational studies, that the pulverized rocks were created essentially by mechanical processes associated with faulting.

5.1. Generating mechanisms of the pulverized rock

The properties of pulverized rocks and the spatial locations where they are observed have led to several hypotheses on their generating mechanism. The structural context indicates they are clearly associated with faulting; intense fracturing close to the fault core results in angular grain fragments down the micron scale (Fig. 6h), and a decrease in the degree of pulverization with increasing distance from the fault (e.g. Fig. 5). The observations of Wilson et al. (2005) at Tejon Pass showed that the rock mass consisted of a diffuse abundance of tension features and considerable reduction of grain size, while still maintaining the original rock fabric as we have described on the ATTL granites. Rockwell et al. (2009) showed similarly that in thin section most grains are intensely comminuted, but the original grain boundaries are still visible; in essence highly fractured fragments which interlock with each other. These observations suggest that the original protolith was subjected to large tensional stresses, potentially due to dynamic reduction of normal stress associated with slip during earthquakes along the San Andreas Fault. On the ATTL, the apparent expansion shown by relatively wide and open microfractures (e.g. Fig. 6c, d) as well as the evidence for shattering indicates that these rocks may have formed under such tensile stress conditions, which agrees well with observations of pulverized rocks seen on the San Andreas Fault system in southern California (Dor et al., 2006a; Dor et al., 2009; Rockwell et al., 2009).

Brune et al. (1993) observed in laboratory experiments with foam rubber blocks that as a rupture passes a point on a fault, there is a significant reduction in normal stress due to vibrations normal to the interface and separation during fault slip. Following fieldwork on the SAF, Brune (2001) suggested that such vibrations of normal stress during earthquake slip at seismogenic depth may be responsible for the generation of pulverized rocks. In this and other cases associated with dynamic reduction of normal stress, earthquake slip may occur under lower shear resistance than predicted by the static friction coefficient of many rocks (Byerlee, 1978). The latter, in turn, has considerable significance for a variety of important issues concerning earthquake mechanics (see, e.g., Ben-Zion, 2001).

Following the proposition of Brune (2001), Reches and Dewers (2005) proposed that fault gouge could be formed by rock pulverization within the tip region of a fast propagating earthquake due to the intensity of stress and rates of strain in the process zone. They suggested that near the tip of mode II dynamic shear fractures propagating close to the limiting Rayleigh wave velocity there are high tensile stresses and strain rates, alternating between volumetric expansion and contraction and producing narrow zones of pulverized rock gouge. While the proposed mechanisms of Brune (2001) and Reches and Dewers (2005) can produce large dynamic tensional stresses needed to create such rock fabric, they fail to account for the fact that pulverized rocks are commonly found primarily only one side of a fault core or primary slip zone. The same shortcoming applies to other proposed mechanisms for dynamic reductions of normal stress during earthquake rupture including acoustic fluidization (Melosh, 1979) and a variety of fluid effects (Byerlee, 1993; Miller et al., 1996; Rice, 1992). Acoustic fluidization and fluid effects are not expected to produce high pervasive rock damage on a scale of 100–300 m. In addition, collisions of rough surfaces are expected to increase the width of the slip zone with increasing slip due to fractal-like irregularities (e.g. Power and Tullis, 1991; Scholz and Aviles, 1986). This is not consistent with the observations on the ATTL, where the majority of the ~17 km fault slip (Maruyama & Lin, 2002) occurred within a localized fault core up to ~10 cm in width. Similar high slip localizations are commonly observed on other large strike-slip faults (e.g., Chester et al., 1993; Chester et al., 2004; Lockner et al., 2000; Rockwell and Ben-Zion, 2007; Sibson, 2003; Smith et al. 2011; Wibberley and Shimamoto, 2003).

Another possible mechanism for pulverized rock genesis is based on dynamic ruptures on fault bimaterial interfaces (Ben-Zion and Shi, 2005). Analytical results and numerical simulations show that the strain incompatibility associated with the material contrast across the fault produces strong dynamic changes of normal stress near the tips of mode II ruptures (e.g., Adams, 1995; Andrews and Ben-Zion, 1997; Ben-Zion, 2001; Ranjith and Rice, 2001; Weertman, 1980). Behind the tip propagating in the direction of particle motion on the slow velocity side of the fault (referred to as the “preferred direction”) the compressive normal stress drops dynamically and can reverse sign leading to local transient tension (e.g. Ben-Zion and Huang, 2002; Dalguer and Day, 2009). In contrast, behind the tip propagating in the opposite direction the normal stress becomes more compressive leading to dynamic increase of fault strength. The opposite senses of dynamic changes of normal stress in the crack tips propagating in the opposite along-strike directions lead, for wide ranges of friction, initial stress and material contrast conditions, to the development of predominately unidirectional ruptures on the bimaterial interface (e.g., Ampuero and Ben-Zion, 2008; Ben-Zion and Andrews, 1998; Brietzke et al., 2009; Shi and Ben-Zion, 2006). Propagation in the preferred direction is associated with relative or absolute tensile stress near the crack tip, strong dynamic weakening and little heat generation (e.g. Andrews and Ben-Zion, 1997; Ben-Zion and Huang, 2002; Brietzke and Ben-Zion, 2006; Dalguer and Day, 2009).

Repeating occurrence of such ruptures on large strike-slip faults having high angle to the maximum compressive background stress is expected to produce signficantly more damage on the side with faster seismic velocities (Ben-Zion and Shi, 2005). For angles of the maximum compressive stress shallower than about 20°, which may characterize thrust fault environments, the side where most damage is produced changes to the block with lower seismic velocity (Templeton and Rice, 2006, 2008). The width of the dynamically generated intense damage zone is expected to correlate with the slip velocity and length of the rupture pulse on the bimaterial interface (Ben-Zion and Shi, 2005), and may be on the order of hundreds of meters or more. The ATTL is likely to have high angle to the compressive background stress, as in-situ stress measurements in the nearby Nojima–Hirabayashi borehole drilled into the Nojima fault show the orientation of maximum horizontal compression to be north–west–south–east (Ikeda et al., 2001). This is typical for many large strike-slip faults (e.g., Ben-Zion, 2001; Hickman, 1991, and references therein). While the large scale fault zone seismic velocities on the ATTL are currently unknown, the ultrasonic lab measurements of Fig. 10 indicate that the granite has the fastest seismic velocities at depth.

Doan and Gary (2009) showed in a split-bar Hopkinson apparatus that the generation of pulverized fault rocks using initially intact granites collected from the SAF may require very high strain rates ($>150\ s^{-1}$) accommodated in very small strains typical of pulverized rocks. They suggested that the high strain rates producing the observed pulverized rocks are generated by supershear ruptures. However, theoretical studies indicate that the generation of

supershear ruptures requires both higher and more uniform initial shear stress than those producing regular subshear ruptures (e.g. Zheng and Rice, 1998). This, and the bulk of seismological observations suggest that supershear ruptures are not the common mode of earthquake failure. In addition, the supershear rupture mechanism does not account for the fact that pulverized rocks are observed

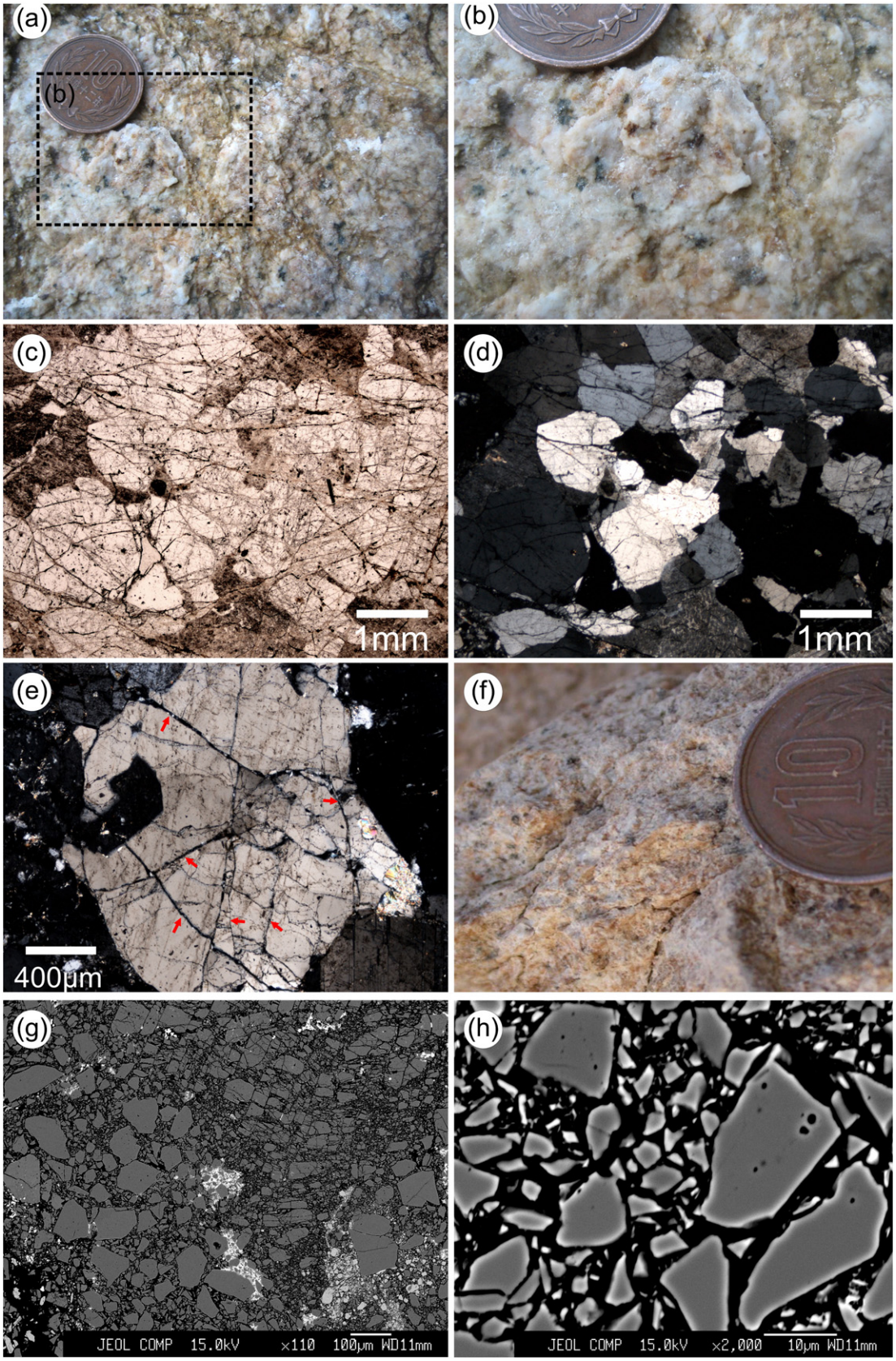

primarily on the side of the fault with faster seismic velocities. Ben-Zion (2001) showed with analytical results on dynamic stress fields that during rupture propagation on a bimaterial interface the slip rate can reach 15–30 m/s. In numerical simulations with purely elastic materials, that do not account for off-fault damage generation, the dynamic slip rates on bimaterial interfaces are considerably higher than the forgoing analytical estimates (Ben-Zion and Huang, 2002; Dalguer and Day, 2009). Such high slip rates on the bimaterial interface between the granite and rhyolite are expected to produce very high strain rates in the near-fault environment. It is thus more likely that the mechanism that generated the pulverized rocks is repeating occurrence of bimaterial ruptures which produce simultaneously strong dynamic reduction of normal stress, high strain rate and statistically preferred propagation direction. Recent observational support for statistically preferred propagation direction of earthquakes on bimaterial faults come from a study of earthquake directivities in the Parkfield section of the SAF (Lengliné and Got (2011)) and analysis of symmetry properties of aftershock sequences along 25 faults in California (Zaliapin and Ben-Zion, 2011).

It may be possible that the asymmetrical pulverization found across the ATTL is not related to rupture events. While the ATTL is smooth in the direction of slip in the fault core at the scale of this study, large scale faults have fractal-type irregularities (Power and Tullis, 1991), and with increasing displacement the damage zone will inevitably grow to accommodate the irregularity misfits, scaling the damage zone size with increasing fault slip and wear (Mitchell and Faulkner, 2009; Wilson et al., 2003). A slight bend in the ATTL to the east of the outcrop area studied has created some open fractures channeling hydrothermal fluids from depth to the surface, but these structures remain in close proximity to the fault core, and the later stage secondary faulting recorded in the study area is likely to postdate the majority of the pulverized rock textures. As discussed by Dor et al. (2006a), however, the rockmass on both sides of the fault should have had a chance to interact with local geometrical complexities, so the irregularity misfits are expected to produce an overall macroscopically symmetric damage in contrast with our observations. In addition, any form of local compression around the fault zone cannot explain the unique textural features of the pulverized rocks present on the ATTL.

5.2. Comparisons to other faults and implications for rupture directivity

South of the ATTL on the Awaji Island, following the 1995 Kobe earthquake, boreholes drilled into the Nojima fault zone revealed some interesting contrasts between the ATTL and the Nojima fault structures (Kobayashi et al., 2001; Lin et al., 2001; Ohtani et al., 2001). The Nojima fault at depth (at least where drilled) has granitic rock of similar age to the Rokko granites (Fig. 1) on both sides of the main fault trace (Kobayashi et al., 2001; Ohtani et al., 2001), in contrast to the granite juxtaposed against rhyolite on the studied section of the ATTL. Observations made on surface outcrops and in shallow (<500 m) drill holes (e.g. Lin et al., 2001), while showing fault breccias and some damage asymmetry, do not show examples of pulverized rocks. For deeper parts of the Nojima fault where both sides of the fault consist of similar granitic rock, pulverized rocks are not reported judging by the detailed descriptions of drill cores (Kobayashi et al., 2001; Ohtani et al., 2001). While weakly deformed and altered, there are no examples of intense asymmetric fault damage and unique pulverized textures on the scale of that seen on the ATTL, and total fault zone thickness is considerably smaller (<50 m—see (Ohtani et al., 2001)) than that of the ATTL pulverized rocks. Moreover, rocks with similar features to those of pulverized rocks as described do not exist in Nojima fault zone. The Nojima fault is regarded as active as the ATTL (Active Fault Research Group, 1991), and hence represents damage from multiple earthquake events. Therefore, the lack of pulverized rocks in the Nojima fault zone which does not separate differing rock types (no material contrast), is an important observation, adding credence to the inference of ATTL pulverized rock genesis due to repeated rupture on a bimaterial interface.

The tendency of bimaterial ruptures to evolve with propagation distance toward strongly asymmetric cracks or unidirectional pulses (e.g., Ampuero and Ben-Zion, 2008; Brietzke et al., 2009; Dalguer and Day, 2009) has important implications for the spatial distribution of the shaking seismic hazard. If the asymmetric pulverized rocks on the Rokko strand of the ATTL are indeed a signature of bimaterial ruptures, as our results appear to be most consistent with, they may reflect a statistically preferred propagation direction towards the East. Trench surveys of the ATTL have revealed three events in the last 3000 years with the recurrence intervals of 1000 and 2000 years (see summary of (The Research Group for Active Faults of Japan, 1991)). The last event was nearly contemporaneous with the 1596 destructive Keicho-Fushimi earthquake (approximate magnitude of M7.5) although other active fault(s) might have moved simultaneously. This earthquake generated asymmetric distribution of shaking intensities consistent with more vigorous rupture to the east (Usami, 2003), in agreement with our inference based on the strong asymmetry of pulverized rock (Figs. 2–6) and laboratory measurements of seismic velocities (Fig. 10).

6. Conclusions

The distinct textural and spatial characteristics of the pulverized rock on the ATTL share many similarities with existing well-documented observations of pulverized granitic rocks previously described in association with several other large strike-slip faults (e.g., Dor et al., 2006a; Rockwell et al., 2009). The pulverized rocks reside only on one side of the fault, the side with higher seismic velocity at conditions corresponding to seismogenic depth. They consist of a diffuse abundance of tension fractures and considerable reduction of grain size into angular fragments down to the micron range, while still maintaining the original grain boundaries and rock fabric. A general apparent lack of significant shear strain suggest that the rocks appear to have been shattered in situ, supported by a lack of evidence for grain fragment rotation, wear and rounding of fragments which are characteristic features of fault rocks such as a fault breccia and cataclasite. These observations suggest that the original protolith was subjected to strong tensional stresses. The observed microfracture damage heavily dominates over macrofracture damage, and there is a clear decrease in microfracture damage with increasing distance from the fault confirming these structures are fault related.

Fault rocks observed both on the surface and in deep boreholes around the nearby Nojima fault where similar granitic rock to that of the ATTL occurs on either side of the fault do not show such pulverized rock, suggesting that pulverized rocks are unique to fault zones with prominent bimaterial interfaces. At present, the dynamic stress fields

Fig. 6. (a) Outcrop of pulverized rock around 5 m from the fault core. This was sampled just to the left of the outcrop shown in Fig. 4a. (b) Zoom in of area highlighted in (a), showing original igneous texture preserved. Entire grains can be easily identified, yet the rock remains incohesive due to the intense level of microfracturing. (c) Plane polarized light section of pulverized rock taken around 25 m from the fault core. (d) Crossed polarized view of (c). (e) Sample taken from around 50 m from the fault, in cross polarized light. Opening mode tension cracks can be seen (with some examples arrowed in red), as well as a lack of rotation showing all segments going into extinction at the same time. (f) Macroscopic view of pulverized rock showing original igneous texture at 50 m from the fault.(g) Scanning electron microscope image of more intensively pulverized samples taken from within the first few meters from beginning of the pulverized zone. (h) Scanning electronic microscope image showing angular particles down to the micron scale. Taken from the same samples as (g).

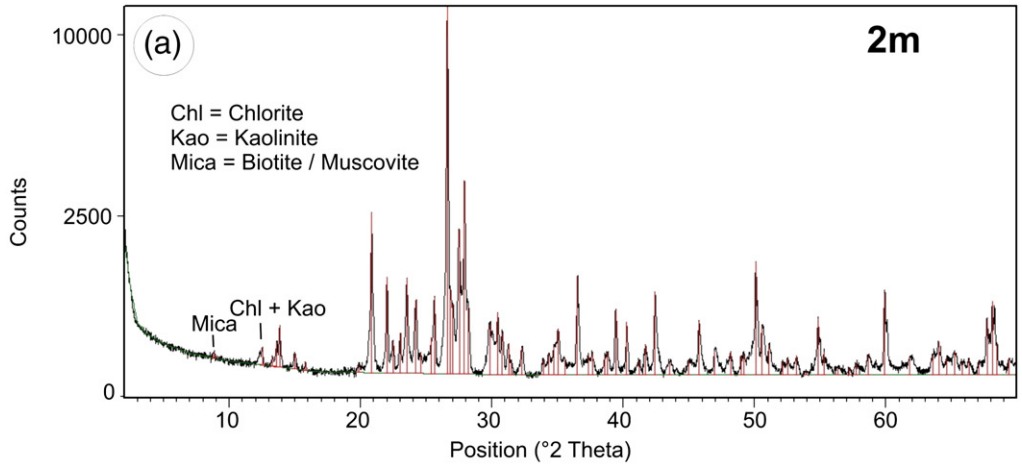

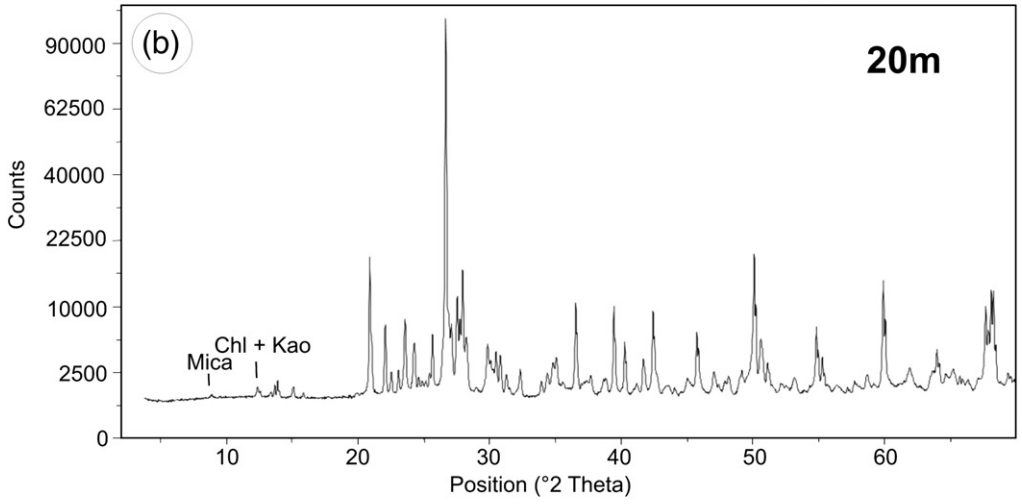

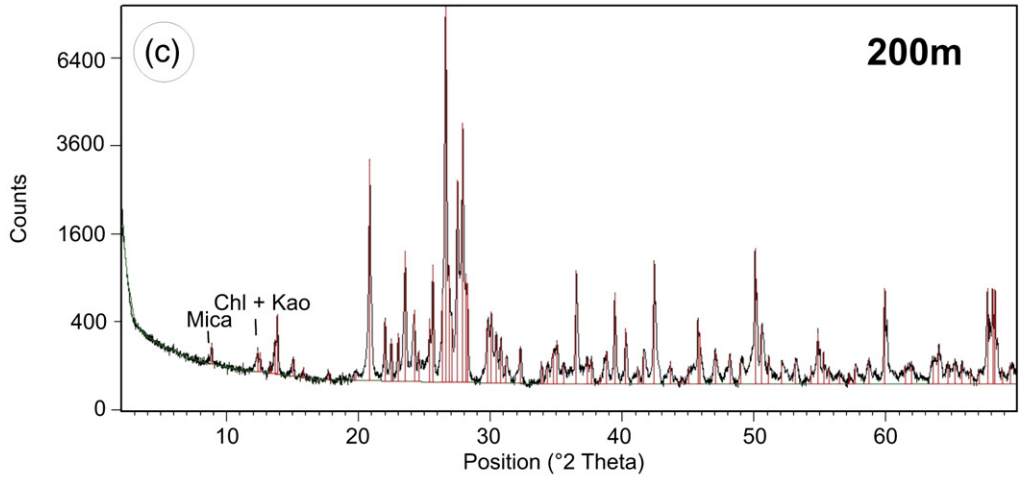

(d)

Mineral	2m	20m	200m
Quartz	42%	45%	36%
K-feldspar	16%	21%	18%
Plagioclase (albite)	39%	27%	43%
Chlorite	0 %	2%	0 %
Phyllosilicates	< 5%	< 5%	< 5%

Fig. 7. (a) XRD diffractogram at low angle on sample taken from 2 m from the fault. Note Y-axis is Log scale and Cu Kα radiation used.(b) XRD diffractogram at low angle on sample taken from 20 m from the fault. Note Y-axis is Log scale and Cu Kα radiation used.(c) Comparison diffractogram at low angle. Note Y-axis is Log scale and Cu Kα radiation used. (d) Comparison of mineral compositions for samples shown in (a)–(c).

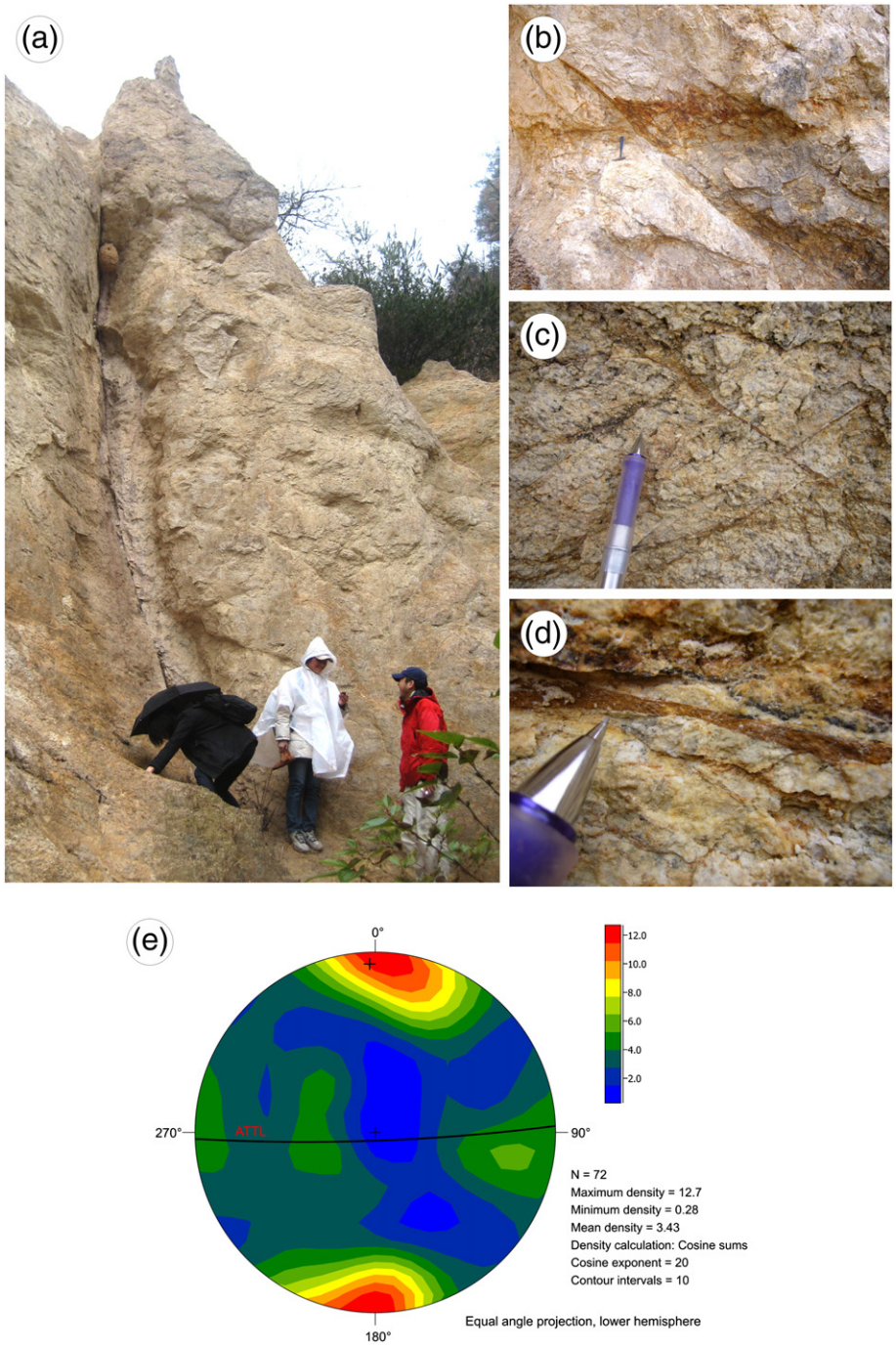

Fig. 8. (a) Subsidiary fault ~10 m from the fault core, with a localized gouge zone up to 5 cm in width. This fault appears to be a splay fault from the main ATTL trace. (b) Subsidiary fault ~100 m from the fault core. (c) Example of small scale displacement on fractures close to subsidiary faults. (d) Example of iron-rich fault vein, typical of many subsidiary faults. (e) Lower hemisphere equal angle stereonet projections showing poles to planes of all subsidiary faults (Ntot = 72) in the pulverized rocks of the Hakusui-Kyo outcrop. Great circle represents the orientation of the ATTL.

produced by repeating occurrences of earthquake ruptures on the granite/rhyolite bimaterial interface in the ATTL appear to provide the most consistent explanation for the set of available observations. To further test these conclusions, larger scale seismic velocity measurements should be made to image the velocity structure of the ATTL at depth, and more mapping along the strike of the ATTL are needed to better characterize the spatial extent of pulverized rocks. Additional constrained experimental studies such as those at high strain rates recreating repeated rupture events need to be designed, in order to provide more stringent tests for the generating mechanism. Detailed work on grain size distribution measurements on these rocks will have important implications for the amount of fracture energy and type of stress field responsible for producing the observed damage.

Acknowledgments

We thank James Utley (University of Liverpool), Giulio Di Toro and Federico Zorzi (Padua University) for providing some additional semi-quantitative XRD data. The paper benefitted from constructive

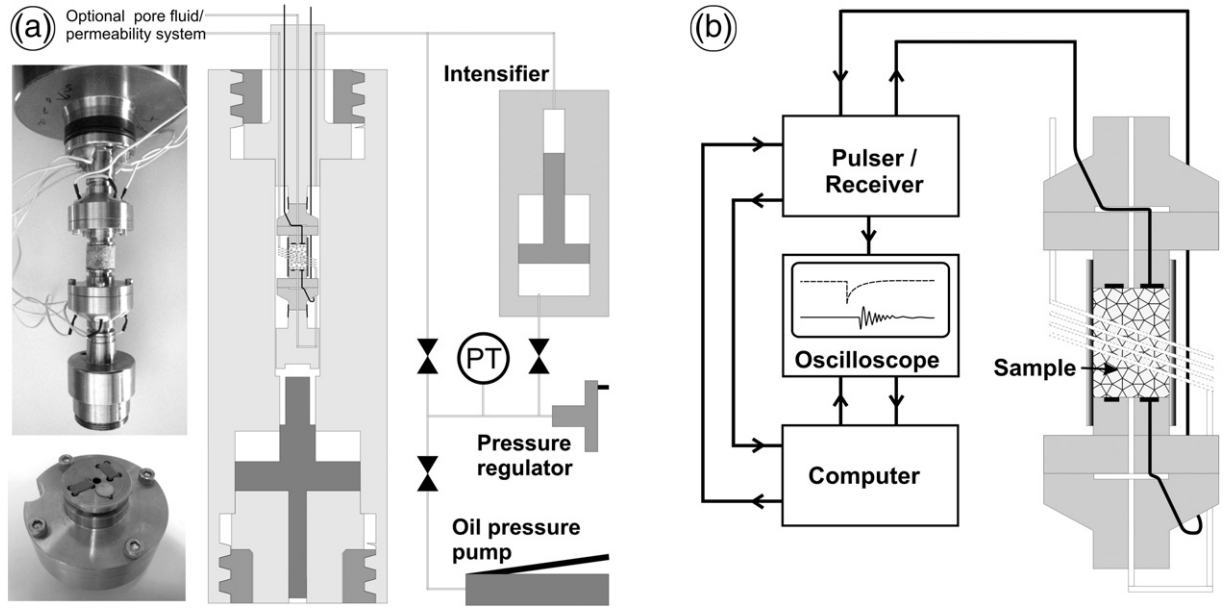

Fig. 9. (a) Schematic diagram illustrating the experimental configuration of a confined sample up to 100 MPa. Confining pressure is generated by an oil pressure hand pump, and kept constant at the desired value by the pressure regulator. Photos on the left show the sample setup with velocity transducer cells which allow the P and S wave velocity to be measured. (b) Detailed schematic diagram of the cell assembly and the ultrasonic method employed.

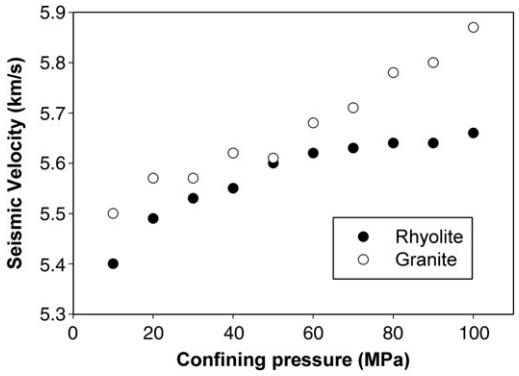

Fig. 10. P wave velocity measurements on intact rhyolite and granite as a function of increasing confining pressure.

comments by Andrea Billi and an anonymous referee. The study was partially funded by a JSPS Research Fellowship awarded to TMM.

References

Adams, G.G., 1995. Self-excited oscillations of two elastic half-spaces sliding with a constant coefficient of friction. J. Appl. Mech.-T. Asme 62, 867–872.
Ampuero, J.P., Ben-Zion, Y., 2008. Cracks, pulses and macroscopic asymmetry of dynamic rupture on a bimaterial interface with velocity-weakening friction. Geophysical Journal International 173, 674–692.
Anders, M.H., Wiltschko, D.V., 1994. Microfracturing, paleostress and the growth of faults. Journal of Structural Geology 16, 795–815.
Andrews, D.J., Ben-Zion, Y., 1997. Wrinkle-like slip pulse on a fault between different materials. Journal of Geophysical Research-Solid Earth 102, 553–571.
Ben-Zion, Y., 2001. Dynamic ruptures in recent models of earthquake faults. Journal of the Mechanics and Physics of Solids 49, 2209–2244.
Ben-Zion, Y., Andrews, D.J., 1998. Properties and implications of dynamic rupture along a material interface. Bulletin of the Seismological Society of America 88, 1085–1094.
Ben-Zion, Y., Huang, Y., 2002. Dynamic rupture on an interface between a compliant fault zone layer and a stiffer surrounding solid. Journal of Geophysical Research-Solid Earth 107, 2042.
Ben-Zion, Y., Shi, Z.Q., 2005. Dynamic rupture on a material interface with spontaneous generation of plastic strain in the bulk. Earth and Planetary Science Letters 236, 486–496.
Blenkinsop, T.G., 1991. Cataclasis and processes of particle-size reduction. Pure and Applied Geophysics 136, 59–86.
Brietzke, G.B., Ben-Zion, Y., 2006. Examining tendencies of in-plane rupture to migrate to material interfaces. Geophysical Journal International 167, 807–819.
Brietzke, G.B., Cochard, A., Igel, H., 2009. Importance of bimaterial interfaces for earthquake dynamics and strong ground motion. Geophysical Journal International 178, 921–938.
Brune, J.N., 2001. Fault normal dynamic loading and unloading: an explanation for "non-gouge" rock powder and lack of fault-parallel shear bands along the San Andreas Fault. EOS Trans. Am. Geophys. Union 82 (Abstract. #S22B-0655).
Brune, J.N., Brown, S., Johnson, P.A., 1993. Rupture mechanism and interface separation in foam rubber models of earthquakes—a possible solution to the heat-flow paradox and the paradox of large overthrusts. Tectonophysics 218, 59–67.
Byerlee, J., 1978. Friction of rocks. Pure and Applied Geophysics 116, 615–626.
Byerlee, J., 1993. Model for episodic flow of high-pressure water in fault zones before earthquakes. Geology 21, 303–306.
Chester, F.M., Evans, J.P., Biegel, R.L., 1993. Internal structure and weakening mechanisms of the San-Andreas Fault. Journal of Geophysical Research-Solid Earth 98, 771–786.
Chester, F.M., Chester, J.S., Kirschner, D.L., Schulz, S.E., Evans, J.P., 2004. Structure of large-displacement, strike-slip fault zones in the brittle continental crust. In: Karner, G.D., Taylor, B., Driscoll, N.W., Kohlstedt, D.L. (Eds.), Rheology and Deformation in the Lithosphere at Continental Margins. Columbia Univ. Press, New York, pp. 223–260.
Dalguer, L.A., Day, S.M., 2009. Asymmetric rupture of large aspect-ratio faults at bimaterial interface in 3D. Geophysical Research Letters 36. doi:10.1029/2009GL040303.
Di Toro, G., Nielsen, S., Pennacchioni, G., 2005a. Earthquake rupture dynamics frozen in exhumed ancient faults. Nature 436, 1009–1012.
Di Toro, G., Pennacchioni, G., Teza, G., 2005b. Can pseudotachylytes be used to infer earthquake source parameters? An example of limitations in the study of exhumed faults. Tectonophysics 402, 3–20.
Doan, M.L., Gary, G., 2009. Rock pulverization at high strain rate near the San Andreas Fault. Nat. Geosci. 2, 709–712.
Dor, O., Ben-Zion, Y., Rockwell, T.K., Brune, J., 2006a. Pulverized rocks in the Mojave section of the San Andreas Fault Zone. Earth and Planetary Science Letters 245, 642–654.
Dor, O., Rockwell, T.K., Ben-Zion, Y., 2006b. Geological observations of damage asymmetry in the structure of the San Jacinto, San Andreas and Punchbowl faults in Southern California: a possible indicator for preferred rupture propagation direction. Pure and Applied Geophysics 163, 301–349.
Dor, O., Yildirim, C., Rockwell, T.K., Ben-Zion, Y., Emre, O., Sisk, M., Duman, T.Y., 2008. Geological and geomorphologic asymmetry across the rupture zones of the 1943 and 1944 earthquakes on the North Anatolian Fault: possible signals for preferred earthquake propagation direction. Geophysical Journal International 173, 483–504.
Dor, O., Chester, J.S., Ben-Zion, Y., Brune, J.N., Rockwell, T.K., 2009. Characterization of damage in sandstones along the Mojave section of the San Andreas Fault: implications for the shallow extent of damage generation. Pure and Applied Geophysics 166, 1747–1773.
Hickman, S.H., 1991. Stress in the lithosphere and the strength of active faults. Rev. Geophys. 29, 759–775.

Huzita, K., Kasama, T., 1982. Geology of Osaka–Seihokubu district. Quadrangle series (112 pp.) Geol. Surv. Jpn. 1, 50,000 (in Japanese with English abstract).
Huzita, K., Kasama, T., 1983. Geology of Kobe district. Quadrangle series (115 pp.) Geol. Surv. Jpn. 1, 50,000 (in Japanese with English abstract).
Ikeda, R., Iio, Y., Omura, K., 2001. In situ stress measurements in NIED boreholes in and around the fault zone near the 1995 Hyogo-ken Nanbu earthquake, Japan. Island Arc. 10, 252–260.
Kobayashi, K., Hirano, S., Arai, T., Ikeda, R., Omura, K., Sano, H., Sawaguchi, T., Tanaka, H., Tomita, T., Tomida, N., Matsuda, T., Yamazaki, A., 2001. Distribution of fault rocks in the fracture zone of the Nojima Fault at a depth of 1140 m: observations from the Hirabayashi NIED drill core. Island Arc. 10, 411–421.
Lengliné, O., Got, J.-L., 2011. Rupture directivity of microearthquake sequences near Parkfield, California, Geophys. Res. Lett. 38, L08310. doi:10.1029/2011GL047303.
Lewis, M.A., Peng, Z., Ben-Zion, Y., Vernon, F.L., 2005. Shallow seismic trapping structure in the San Jacinto fault zone near Anza, California. Geophysical Journal International 162, 867–881.
Lewis, M.A., Ben-Zion, Y., McGuire, J., 2007. Imaging the deep structure of the San Andreas Fault south of Hollister with joint analysis of fault-zone head and direct *P* arrivals. Geophysical Journal International 169, 1028–1042.
Lin, A.M., Shimamoto, T., Maruyama, T., Sigetomi, M., Miyata, T., Takemura, K., Tanaka, H., Uda, S., Murata, A., 2001. Comparative study of cataclastic rocks from a drill core and outcrops of the Nojima Fault zone on Awaji Island, Japan. Island Arc. 10, 368–380.
Lockner, D.A., Naka, H., Tanaka, H., Ito, H., Ikeda, R., 2000. Permeability and strength of core samples from the Nojima fault of the 1995 Kobe earthquake. GSJ Internal Report No. EQ/00/1, Proceedings of the Internal Workshop on Nojima Fault Core and Borehole Date Analysis, pp. 147–157.
Maruyama, T., Lin, A.M., 2002. Active strike-slip faulting history inferred from offsets of topographic features and basement rocks: a case study of the Arima-Takatsuki Tectonic Line, southwest Japan. Tectonophysics 344, 81–101.
Melosh, H.J., 1979. Acoustic fluidization—new geologic process. Journal of Geophysical Research 84, 7513–7520.
Miller, S.A., Nur, A., Olgaard, D.L., 1996. Earthquakes as a coupled shear stress high pore pressure dynamical system. Geophysical Research Letters 23, 197–200.
Mitchell, T.M., Faulkner, D.R., 2009. The nature and origin of off-fault damage surrounding strike-slip fault zones with a wide range of displacements: a field study from the Atacama fault system, northern Chile. Journal of Structural Geology 31, 802–816.
Ohtani, T., Tanaka, H., Fujimoto, K., Higuchi, T., Tomida, N., Ito, H., 2001. Internal structure of the Nojima Fault zone from the Hirabayashi GSJ drill core. Island Arc. 10, 392–400.
Ozaki, M., Matsuura, H., Sato, Y., 1996. Geologic age of the Kobe Group. J. Geol. Soc. Jpn. 102, 73–83 (in Japanese with English abstract).
Power, W.L., Tullis, T.E., 1991. Euclidean and fractal models for the description of rock surface-roughness. Journal of Geophysical Research-Solid Earth and Planets 96, 415–424.
Ranjith, K., Rice, J.R., 2001. Slip dynamics at an interface between dissimilar materials. Journal of the Mechanics and Physics of Solids 49, 341–361.
Reches, Z., Dewers, T.A., 2005. Gouge formation by dynamic pulverization during earthquake rupture. Earth and Planetary Science Letters 235, 361–374.
Rice, J.R., 1992. Fault stress states, pore pressure distributions, and the weakness of the San Andreas Fault. In: Evans, B., Wong, T.-F. (Eds.), Fault Mechanics and Transport Properties in Rocks, 28. Academic Press, pp. 475–503.
Rockwell, T.K., Ben-Zion, Y., 2007. High localization of primary slip zones in large earthquakes from paleoseismic trenches: observations and implications for earthquake physics. Journal of Geophysical Research-Solid Earth 112, B10304.
Rockwell, T., Sisk, M., Girty, G., Dor, O., Wechsler, N., Ben-Zion, Y., 2009. Chemical and physical characteristics of pulverized tejon lookout granite adjacent to the San Andreas and Garlock Faults: implications for earthquake physics. Pure and Applied Geophysics 166, 1725–1746.
Sangawa, A., 1978. Fault topography and Quaternary faulting along the middle and eastern parts of the Arima-Takatsuki Tectonic Line, Kinki district, central Japan. Geogr. Rev. Jpn. 51, 760–775 (in Japanese with English abstract).
Scholz, C.H., Aviles, C.A., 1986. The fractal geometry of faults and faulting. In: Das, S., Boatwright, J., Scholz, C. (Eds.), Earthquake Source Mechanics, 9. Academic Press, New York.
Seno, T., Stein, S., Gripp, A.E., 1993. A model for the motion of the Philippine Sea Plate consistent with Nuvel-1 and geological data. Journal of Geophysical Research-Solid Earth 98, 17941–17948.
Shi, Z.Q., Ben-Zion, Y., 2006. Dynamic rupture on a bimaterial interface governed by slip-weakening friction. Geophysical Journal International 165, 469–484.
Shimamoto, T., 2003. Development of an intravessel deformation and fluid-flow apparatus,'Yoko'. The 110th Annual Meeting of the Geological Society of Japan, O-228.
Sibson, R.H., 1975. Generation of pseudotachylyte by ancient seismic faulting. Geophysical Journal of the Royal Astronomical Society 43, 775–792.
Sibson, R.H., 1977. Fault rocks and fault mechanisms. Journal of the Geological Society 133 (3), 191–213.
Sibson, R.H., 2003. Thickness of the seismic slip zone. Bulletin of the Seismological Society of America 93, 1169–1178.
Smith, S., Billi, A., Toro, G., Spiess, R., 2011. Principal slip zones in limestone: microstructural characterization and implications for the seismic Cycle (Tre Monti Fault, Central Apennines, Italy). Pure and Applied Geophysics 1–27. doi:10.1007/s00024-011-0267-5.
Templeton, E.L., Rice, J.R., 2006. Extent and distribution of off-fault plasticity during seismic rupture including bimaterial effects. Eos Trans. AGU 87 (52) (Fall Meet. Suppl., Abstract S34A-01).
Templeton, E.L., Rice, J.R., 2008. Off-fault plasticity and earthquake rupture dynamics: 1. Dry materials or neglect of fluid pressure changes. Journal of Geophysical Research-Solid Earth 113, B09306.
Teranishi, K., Isomura, K., Yano, M., Tsuji, H., Chayama, K., Fujiwara, S., Yao, K., Utida, H., 2003. Measurement of distribution of rare earth elements in Arima-type springs using preconcentration with chelating resin/ICP-MS. Bunseki Kagaku 52, 289–296.
The Research Group for Active Faults of Japan, 1991. Active Faults of Japan: sheet maps and inventories, revised edition, University of Tokyo Press, (437pp.).
Usami, T., 2003. A catalogue of disastrous earthquakes in Japan. (in Japanese) updated edition. University of Tokyo Press. (728pp.).
Wechsler, N., Rockwell, T.K., Ben-Zion, Y., 2009. Application of high resolution DEM data to detect rock damage from geomorphic signals along the central San Jacinto Fault. Geomorphology 113, 82–96.
Weertman, J., 1980. Unstable slippage across a fault that separates elastic media of different elastic-constants. Journal of Geophysical Research 85, 1455–1461.
Wibberley, C.A.J., Shimamoto, T., 2003. Internal structure and permeability of major strike-slip fault zones: the Median Tectonic Line in Mie Prefecture, Southwest Japan. Journal of Structural Geology 25, 59–78.
Wilson, J.E., Chester, J.S., Chester, F.M., 2003. Microfracture analysis of fault growth and wear processes, Punchbowl Fault, San Andreas System, California. Journal of Structural Geology 25, 1855–1873.
Wilson, B., Dewers, T., Reches, Z., Brune, J., 2005. Particle size and energetics of gouge from earthquake rupture zones. Nature 434, 749–752.
Zaliapin, I., Ben-Zion, Y., 2011. Asymmetric distribution of aftershocks on large faults in California, Geophys. J. Int. 185, 1288–1304. doi:10.1111/j.1365-246X.2011.04995.x.
Zheng, G., Rice, J.R., 1998. Conditions under which velocity-weakening friction allows a self-healing versus a cracklike mode of rupture. Bulletin of the Seismological Society of America 88, 1466–1483.